

Site response analysis of Vartholomio W-Greece from singular spectrum analysis of microtremor and weak motion data

G-Akis Tselentis, Paraskevas Paraskevopoulos *

Patras Seismological Laboratory, University of Patras, Greece

ARTICLE INFO

Article history:

Received 28 August 2009

Received in revised form

11 December 2009

Accepted 15 December 2009

Keywords:

Site effects

Microtremors

Weak motion

Singular spectrum analysis

Amplification

Vartholomio

ABSTRACT

Twenty six sites were instrumented in the city of Vartholomio following the December 2, 2002 Ms 6.0 earthquake. Thirty weak events from the aftershock sequence as well as microtremors were used to identify amplifications due to geological site effects. Horizontal-to-vertical spectral ratios (HVS—Nakamura estimates) and weak events ratios were calculated and the singular spectrum analysis (SSA) method was used. The results showed that the effects of SSA on the stability of the frequency peak and amplitude distribution of HVS for both weak motion and microtremors. The data analysis confirms the role of near surface geology in causing locally significant variations of the predominant frequencies and amplitudes of ground shaking as already inferred from the distribution of damages. The site response spectra exhibited significant peaks within the range of 1.5–2.6 Hz and the amplification factor did not exceed 6.5. Finally the parts of the HVS ratios from ~0.2 up to 10 Hz were used, in order to create an automatic optimal zonation of the study area using a genetic algorithm. This procedure resulted in the division of the city into 2 main zones.

© 2010 Published by Elsevier Ltd.

1. Introduction

Local site conditions are one of the most important factors which characterize the distribution of earthquake damage. Well known examples from San Francisco (1989), Guerrero Michoacan (1985), Northridge (1994), Kobe (1995), Armenia (1999) and Turkey (1999) earthquakes have been extensively cited to illustrate the role of surface geology on seismic waves. Reliable site response models are essential to estimate the amplification potential and the probabilistic and deterministic distributions of the peak and spectral amplitudes of ground shaking at the surface.

Many experimental methods have been used to quantify the site effects and define the site response functions (e.g. Field and Jacob [14]). Although the best determination of site response functions is obtained from strong ground motions [30], spectral analysis of microtremors (low amplitude ground motion continuously recorded when earthquakes are not recorded) and weak motions from earthquakes can be an alternative tool to quantify site effects [2].

The horizontal-to-vertical spectral ratio (HVS) (the ratio between the Fourier amplitude spectra of the horizontal and vertical components of the microtremors) was first introduced by Nogoshi and Igarashi [27] and was widely spread by Nakamura

[24–26]. Since then, many investigators have reported the successful application of the method for estimating the fundamental frequency f_0 , which has been applied also inside urban environments e.g. [3,4,11,13,15,20,29,31]. Furthermore, several studies e.g. [8,33] found that the HVS results are correlated with the distribution of damages, after taking vulnerability into consideration.

Several theoretical 1D investigations that have computed microtremor synthetics using randomly distributed near-surface sources e.g [14,18], have shown that H/V ratios sharply peaked around the fundamental resonance frequency of SH waves whenever the surface layer exhibits a sharp impedance contrast with the underlying stiffer formations.

A simple straightforward modification of the above technique consists in taking the spectral ratio between the horizontal and the vertical components of weak earthquake recordings. This technique is in fact a combination of Langston's [19] receiver function method for determining the velocity structure of the crust from the horizontal to vertical spectral ratio of teleseismic P waves, and Nakamura's method. In the literature several studies can be found where weak motion data were applied to assess site effects in urban areas, even though originally they were not proposed for cities e.g. [10,23,31,32,34,36,38,39] exhibiting a rather good correlation with surface geology, and in many cases are able to predict site resonance frequencies, whereas there is a lower reliability on the amplification factors [2]. Most of the earthquake data examined in the HVS investigations are relevant

* Corresponding author.

E-mail address: paris@upatras.gr (P. Paraskevopoulos).

to weak motion recorded at short term temporary networks deployed for microzonation purposes. To obtain a statistically significant database of weak events we need long recording periods, with the exception if we install the network to record an aftershock sequence, as it is in our case. Theodulidis et al. [34] using a dataset of 22 earthquakes at the Garner Valley array, concluded that the HVSR applied to weak motion data showed good stability and it was not influenced by source location of mechanisms. In another investigation Mucciarelli et al. [23], after analyzing two years worth of data, concluded that HVSR is a remarkably stable site dependant feature.

Recently Carniel et al. [9], showed that the application of the singular spectrum analysis (SSA) methodology on Nakamura's approach can improve the results. The SSA allows the time series to be decomposed into different components, e.g., the signal itself, as well as various noise components, which can be subsequently removed from the time series. Since microtremors and weak motions are measured along two horizontal directions and one vertical direction, we get two Nakamura spectral ratios that in many cases show considerable difference. The cause of this difference may be the presence of artificial noise (e.g. ghost transients) and the application of the SSA methodology can reduce this effect.

Finally in order to identify parts of the study area that have similar ground-motion behavior, an automatic method using genetic algorithms as in [5,6] is employed. This method uses the classification of the HVSRs as objective criteria for an initial microzonation of the area.

2. Geological setting and data

The city of Vartholomio is located in the most seismically active part of Greece, and is undergoing urban development. During its history, strong earthquakes have severely affected the site. On 16 October 1988 an $M_s=5.9$ earthquake reached a seismic intensity of 7 on the MSK scale, causing serious damages in the city. The seismic intensity was higher than would normally be expected from the magnitude and epicentral distance of the

earthquake (Fig. 1). More recently, the $M_s=6$, December 2, 2002 earthquake, severely damaged many parts of the town, reaching a seismic intensity of 5–6 on the MSK scale. It is likely that the structural damages all over the area of Vartholomio, after taking into account the vulnerability of the structures, are caused by local site effects of the sedimentary layer that may have amplified the earthquake ground motion.

Following the December 2, 2002 M_s 6.0 earthquake and during the period from December 7, 2002 to January 7, 2003, the University of Patras seismological lab installed and operated a 26 stations seismological network in and around the city of Vartholomio (Fig. 1). The stations were instrumented with a LandTech LT-S01, three component velocity sensor with flat response between 0.2 and 100 Hz and a sensitivity of 1000 V/m.s. The seismological data have been recorded using an EarthData 24bit digitizer with a sampling rate of 100 samples /second.

The study area is situated on the external part of the Hellenic Arc and therefore subjected to intense neotectonic deformation and high seismicity. More specifically, this area is part of the neotectonic depression (graben) of Pirgos, which is delimited by two faults of NW–SE and NNE–SSW direction and it is characterized by co-sedimentation tectonism [21].

To the west of the city of Vartholomio, there are outcropping alpine formations (Ionian zone). These are considered as the bedrock of Vartholomio. In geochronological order, three geological formations can be located [22]:

The Vounargo formation, having a total thickness that can exceed 500 m, comprises of various sandstones and shales. This formation outcrops to the west of Vartholomio.

Developing unconformably over the previous Vounargo formation, are the Calcitic Sandstones. They contain locally fine or coarser material, from various rocks. This unit has a thickness of up to 20 m.

Alluvial formations, composed of clayey sands and sandy clays, overlying unconformably the previous formation. These occupy the major plain of Vartholomio and their thickness is increasing towards the east.

The topmost layer, inside the city, has a thickness increasing from 6 m in the Western part to 15 m in the Eastern part, and

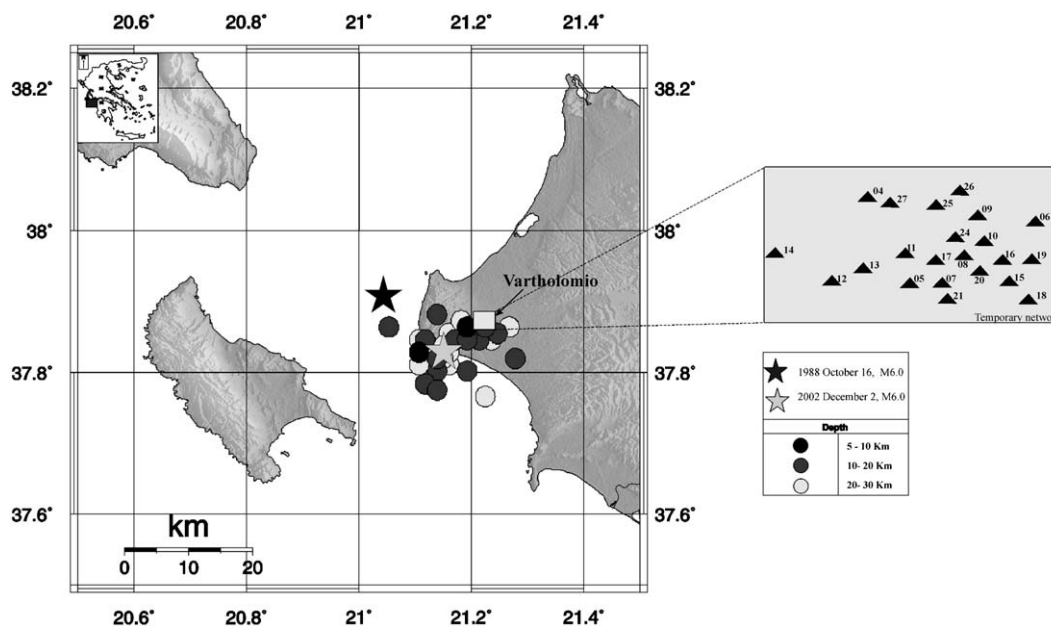


Fig. 1. Epicenters of the $M_s=5.9$ 1988 (black star) and $M_s=6.0$ 2002 (grey star) earthquakes. Triangles depict the installed microearthquake network within the Vartholomio city. Circles are the epicenters of the weak motion data used in the present investigation.

according to research-drillings and geophysical investigations [35], consists of recent deposits of soft to medium density clayey sands, sandy clay of medium cohesiveness, sandy clays of medium plasticity locally with gravel, thin layers of silt and soft layers of plastic clay.

3. Theory

3.1. Singular spectral analysis (SSA) method

The SSA method [12], sometimes called caterpillar method [16] or Karhunen–Loève decomposition [28], has its roots in chaos theory [7] and only recently has been applied to in time series analysis of microtremor data by [9].

SSA is designed to decompose time series and thus provides insight into the unknown or only partially known dynamics of the underlying system that generates the series [37]. It allows one to unravel the information embedded in the delay-coordinate phase space by decomposing the sequence of augmented vectors thus obtained into elementary patterns of behavior. It does so by providing data-adaptive filters that help separate the time series into components that are statistically independent, at zero lag, in the augmented vector space of interest. These components can be classified essentially into trends of oscillatory patterns and noise.

The method provides an orthogonal basis onto which the data can be transformed, thus making individual data components (modes) linearly independent. Each of the orthogonal modes, which are projections of the original data onto new orthogonal basis vectors, is characterized by its variance, which is given by the related eigenvalue of the covariance matrix. In traditional SSA, the distinction of signal from noise is based on finding a threshold to a noise floor in a sequence of eigenvalues given in a descending order.

The first step of SSA is the embedding, where the one-dimensional seismic data time series is recast as a multidimensional trajectory matrix X . Considering a time series $x = \{x_1, x_2, x_3, \dots, x_N\}$ with N samples and an embedding dimension (caterpillar length) M , we obtain the trajectory matrix X

$$X = \begin{bmatrix} x_1 & x_2 & \dots & x_M \\ x_2 & x_3 & \dots & x_{M+1} \\ \dots & \dots & \dots & \dots \\ x_k & x_{k+1} & \dots & x_N \end{bmatrix} \quad (1)$$

where $k = N - M + 1$.

The number of columns of the trajectory matrix should be sufficiently large to capture the global behavior of the time series.

Starting the process we compute the singular value decomposition of X . We start by computing the lagged covariance matrix C

$$C = \frac{X^T X}{N - M} \quad (2)$$

and its spectral decomposition $C = \Phi \Lambda \Phi^T$, where Φ is an orthogonal matrix having as columns the eigenvectors of C (providing the orthonormal Karhunen–Loève basis in the space of vectors x_i), and $\Lambda = \text{diag}(\sigma_1^2, \sigma_2^2, \dots, \sigma_M^2)$ with σ_i^2 non-negative eigenvalues of C giving the variance of orthogonal modes.

The singular value decomposition technique allows obtaining the decomposition of the trajectory matrix as

$$X = USV^T \quad (3)$$

where U is a $(N - M + 1) \times (N - M + 1)$ orthogonal matrix, V is a $m \times m$ orthogonal matrix and S is a $(N - M + 1 \times M)$ diagonal matrix whose elements are the trajectory's matrix singular values which

are equal to the square root of the eigenvalues of C .

$$S = \begin{bmatrix} \sigma_1 & 0 & \dots & 0 \\ 0 & \sigma_2 & \dots & 0 \\ \dots & \dots & \dots & \dots \\ 0 & 0 & \dots & \sigma_m \\ 0 & 0 & \dots & 0 \end{bmatrix} \quad \sigma_1 \geq \sigma_2 \geq \dots \geq \sigma_m \geq 0 \quad (4)$$

Next, we obtain the spectral decomposition of the trajectory matrix

$$X = \sum_{i=1}^m \sigma_i u_i v_i^T = \sum_{i=1}^M X \Phi_i \Phi_i^T \quad (5)$$

where u_i , v_i and Φ_i are U 's, V 's and Φ 's i th columns.

The second processing step is to separate the time series into its signal and noise components, by processing the trajectory matrix over a q -dimensional space

$$X = X_q + \text{noise} = \sum_{i=1}^q \sigma_i u_i v_i^T + \sum_{i=q+1}^M \sigma_i u_i v_i^T = \sum_{i=1}^q X \Phi_i \Phi_i^T + \sum_{i=q+1}^M X \Phi_i \Phi_i^T \quad (6)$$

Thus, the noise-free time series x_q depends on the choice of the parameters M and q with the level of de-noising decreasing with q .

$$Xq = \text{SSA}(x; M, q) \quad (7)$$

In conventional HVSR technique, we obtain two spectral ratios SR_x and SR_y defined as

$$SR_x = \frac{S(x)}{S(z)}, \quad SR_y = \frac{S(y)}{S(z)} \quad (8)$$

where $S(x)$, $S(y)$, $S(z)$ are the corresponding spectra of the seismic recordings along the EW, NS and UD (Up/Down) directions.

Under the hypothesis of a homogeneous and elastic surface layer medium, with planar horizontal layers, the two ratios should be equal, but due to non-ideal conditions the two ratios might be in disagreement, with the SR_x and SR_y peaks not correlating to the same frequencies. The SSA technique can reduce this effect and improve the “matching” between SR_x and SR_y peaks, but in the presence of a laterally non-homogeneous layer this technique can fail, as its success depends on the orientation of the anisotropies with respect to the measurements [1]. In the case of Vartholomio previous extensive geophysical investigations [35], employing shallow reflection refraction and geoelectric surveys have shown that, in general, we can assume a rather planar horizontal layer 1D model that justifies the application of the SSA technique.

Carniel et al. [9] proposed the use of the following spectral ratios

$$SR_x^1 = \frac{S[\text{SSA}(x; M, q_1)]}{S[\text{SSA}(z; M, q_3)]} \quad (9)$$

$$SR_y^1 = \frac{S[\text{SSA}(y; M, q_2)]}{S[\text{SSA}(z; M, q_3)]} \quad (10)$$

where $1 \leq q_1, q_2, q_3 \leq M$

The idea is to find the de-noising level such that the “matching” between the SR_x and SR_y becomes maximum and then select the corresponding q_1, q_2, q_3 by minimizing the quantity

$$\|SR_x^1 - SR_y^1\|^2 = \min \quad (11)$$

Another criterion for choosing the q_1 , q_2 and q_3 is the correlation of the spectral ratios.

$$\text{corr}(SR_x^1 - SR_y^1) = \max \quad (12)$$

or a joint application of the two criteria. As stated in [9] in general the least square function will have better results but the

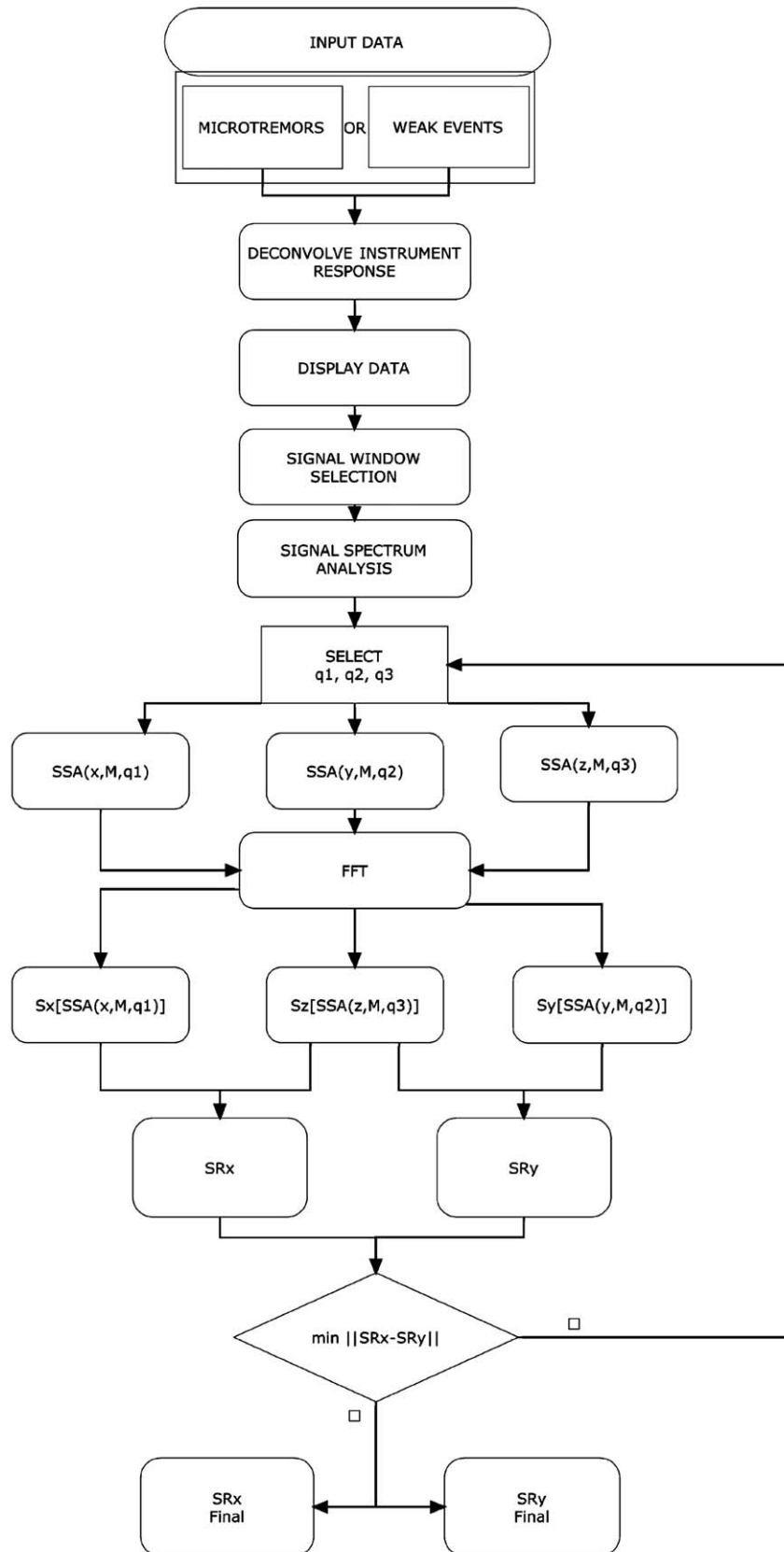


Fig. 2. Data processing stages applied to both microtremor and weak motion data.

correlation could be better suited in the presence of lateral dishomogeneities and difference in amplification factors along the horizontal components.

On selecting the values of q_1 , q_2 and q_3 the following should be taken into account. The value of q_3 should be selected sufficiently high, to avoid false peaks in the ratio. During the selection

process, the results should be monitored for abnormally high peaks that may be present in the resulting ratio and in some cases compared with the non SSA HVSR results. If false peaks are observed a higher value for q_3 should be selected. This was reported in [9] and was also observed during the application of this technique to the data. This is because SSA, as applied, can be considered as a filter keeping only the higher peaks while suppressing the lower ones. This effect becomes less important as the values of q increase. In the case of very small q_3 , the denominator of the ratio is affected and could take very small values causing vertical asymptotes that can in turn produce false peaks in the ratio [9].

A graphical representation of the previous processing stages describing the application of the SSA method is depicted in Fig. 2.

3.2. Zonation using a genetic algorithm

After the SSA processing selected parts of the spectra will be used by a genetic algorithm (GA) in order to produce an automatic zonation of the area. The theory of the method followed is described in greater detail in Braggato et al. [6].

Considering all the N_p stations connected in a Delaunay triangulation, on every station there is a vector $SR_i = (SR_{i,1}, \dots, SR_{i,F})$ whose elements are the values of the spectral ratio computed in the selected frequency range with F the number of frequencies in that range. By removing the edges, the Delaunay triangulation can be partitioned into N_c connected subgraphs each one consisting of N_{p_k} measurement points ($k=1, \dots, N_c$). The edges of the triangulations are weighted using the Euclidean distance of the corresponding HVRS and an Euclidean minimum spanning tree (EMST) is obtained. Then for every connected cluster the within group sum of squares (WGSS) is calculated as described in [6]. This is a measure of the dissimilarity within every cluster. The sum of the WGSSs of all the clusters is called the residual sum of squares (RSS). For a fixed value of N_c , the optimal partitioning, is the one minimizing the value of the RSS.

The optimal zonation depends on finding the optimal value for N_c . A number of statistics can be used as indicators of its value. Following [6] the Bayesian information criterion (BIC) was used.

$$BIC = N_p \ln \left(\frac{RSS}{N_p} \right) + (N_c - 1) \ln(N_p) \quad (13)$$

The N_c selected should minimize the BIC. In this way an N_c is selected that has a small number of clusters, has a low RSS and also achieves a significant reduction in RSS.

As discussed by Bragato and Bressan [5] one disadvantage of using EMSTs is that most partitions of the Delaunay triangulation will not be generated and evaluated. Instead their variable spanning tree (VST) method is used. According to this, for a partition of the triangulation in k connected subsets, $k-1$ edges are selected from the entire triangulation and assigned negative weights. Then employing Kruskal's algorithm the minimum spanning tree that includes them is found. Finally a connected partition of the triangulation is obtained by removing the selected edges from the spanning tree.

For a number of increasing N_c values the genetic algorithm is used to find the optimal partition for a Delaunay triangulation including N_p nodes and N_D edges. During each run, we program the GA using $N_c - 1$ parameters

$$(n_1, n_2, \dots, n_{N_c-1}), \quad 0 \leq n_i \leq N_D - 1 \quad (14)$$

Each n_i represents an edge used to generate the VST. These numbers are encoded as the "chromosomes" of the genetic algorithm, consisting of b bits binary strings each, where b is such that $2^{b-1} < N_D - 1 < 2^b$. The total length of the "chromosomes" is $b(N_c - 1)$ and the search space includes $2^{b(N_c-1)}$ individuals.

After each run the corresponding BIC is calculated. For the value of N_c that BIC becomes minimum, this value is selected. The procedure stops after the minimum is sufficiently individuated.

4. Application of the SSA technique

4.1. Application of the SSA technique on microtremor data

Microtremor recordings have been selected from the installed microearthquake network stations in order to estimate the site effects using the HVSR technique. From the records obtained during the continuous 1 month operation of the microearthquake network, we selected 30 stationary portions of the signal that appear unaffected by strong unwanted signals, such as short transients, small earthquakes or caused by human activities, using windows of 20.48 s length. The spectral analysis included detrending and 5% cosine-tapering before transformation.

Next, the SSA methodology, previously described, was applied (Fig. 2). As the "matching" measure, we choose the least squares sum. For all data sections we first compute the spectrogram for 50% overlapping windows. In this way we can investigate the spectral stability and, if necessary, remove the portions of signals that are clearly contaminated by unwanted signal components, such as those described above. Next, we perform a band-pass filter between 0.2 and 15 Hz. The lowcut frequency is selected in order to remove very high spectral energy in the very low frequency range. Then, for every signal window and every component the SSA decomposition is performed, and the corresponding S_x , S_y and S_z spectral estimates $S[SSA(x;M,q_1)]$, $S[SSA(y;M,q_2)]$ and $S[SSA(z;M,q_3)]$ are obtained (Eqs. (9) and (10)). Finally the ratios of the two horizontal components to the vertical are calculated for every choice of the triplet (q_1, q_2, q_3) and the best HVSRs are selected.

A detailed presentation of the application of the SSA methodology for station Vartholomio 02 is depicted in Fig. 3. Fig. 3a shows an 80 min graph of the vertical component data recordings with the corresponding spectrogram. Next, we select 50% overlapping windows each one consisting of 2048 points. The parts of the signal that display strong (mainly of anthropogenic origin) noise or natural noises (earthquakes) are identified on the time series and the spectrogram and excluded. The excluded part of the signal varied from station to station. After that, the signals are decomposed using the SSA methodology. In order to perform this, taking into account the eigenvalues for every component, an embedding dimension of $M=15$ was chosen. Since this processing is using only the noise reduction and smoothing properties of SSA, the performed tests showed that, if the embedding dimension M is large enough, its exact value was not as important. In order to choose an appropriate value for M , we must get negligible eigenvalues and components must be negligible (Fig. 3b). After determining M the same process is performed for all the overlapping windows and for each component (3×400 windows). Fig. 3b shows the (normalized) SSA decomposition components as well as the eigenvalues for each one, for one randomly selected window.

Next every combination of q_1 , q_2 and q_3 is tried, reconstructing each signal and the corresponding spectra are calculated for every component. For example, for the three components and for every embedding dimension (of the $M=15$) we can obtain M^3 different reconstructions. It is possible after trying all combinations of q_1 , q_2 and q_3 for a few stations and observing the values selected, to limit the range that they can vary in order to reduce the calculation time. Optimal q_1, q_2, q_3 values are selected optimizing the matching between SR_x^i and SR_y^i by minimizing the Euclidean

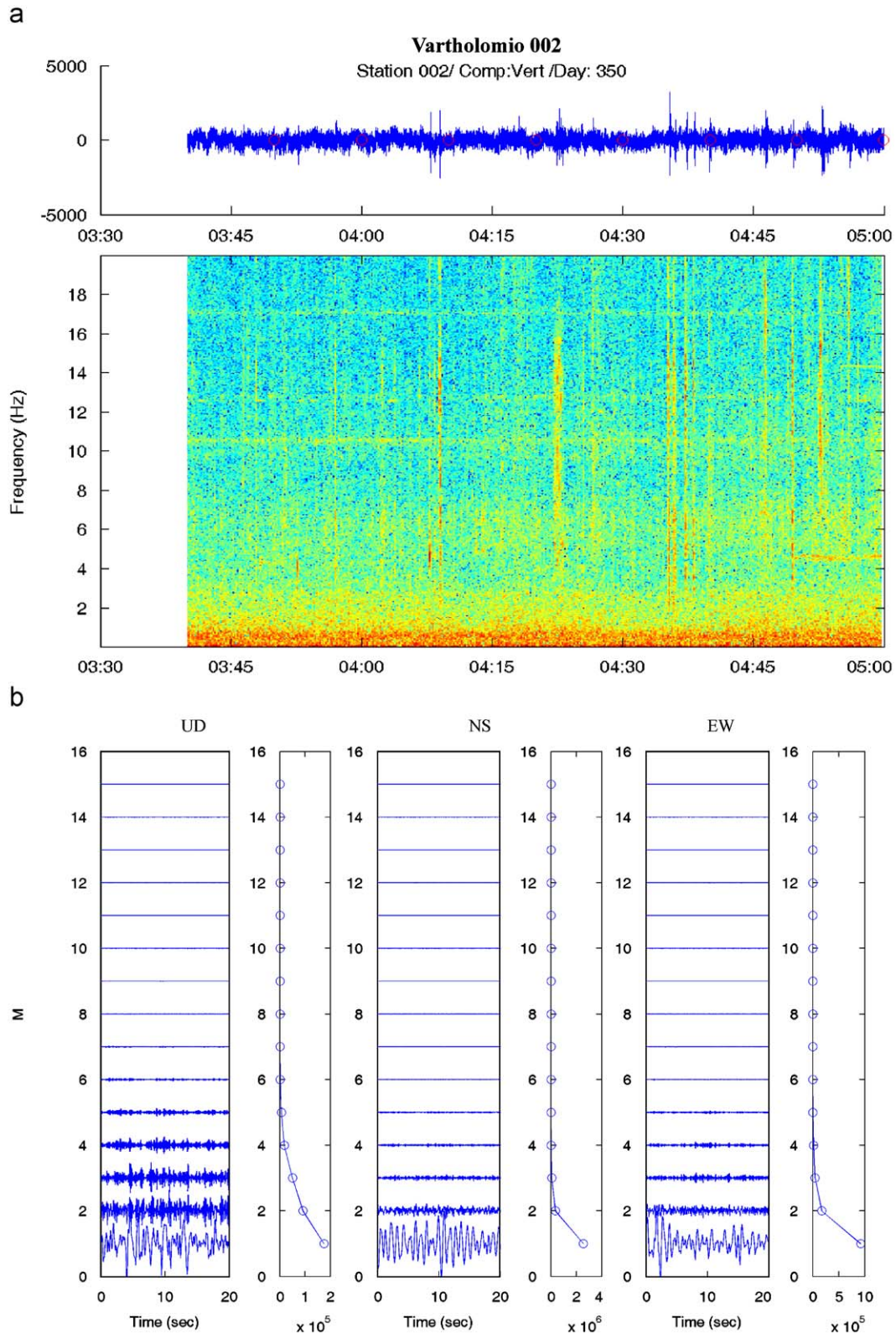


Fig. 3. (a) Example of vertical component recordings with corresponding spectrogram for station 02. (b) SSA normalized decomposition and corresponding eigenvalues.

distance between them (Eq. (11)). In addition SR_x^1 and SR_y^1 are controlled for the presence of false peaks and abnormally high ratio values, as discussed in the theory section. When such peaks are detected, only higher q_3 values are considered for reconstructing the vertical component.

The average spectral ratios without and with the application of the SSA methodology for station 02, are shown in Fig. 4a and 4b, respectively.

To further illustrate the effect of the SSA methodology, Fig. 5 shows the comparison between the average HVSR results of the

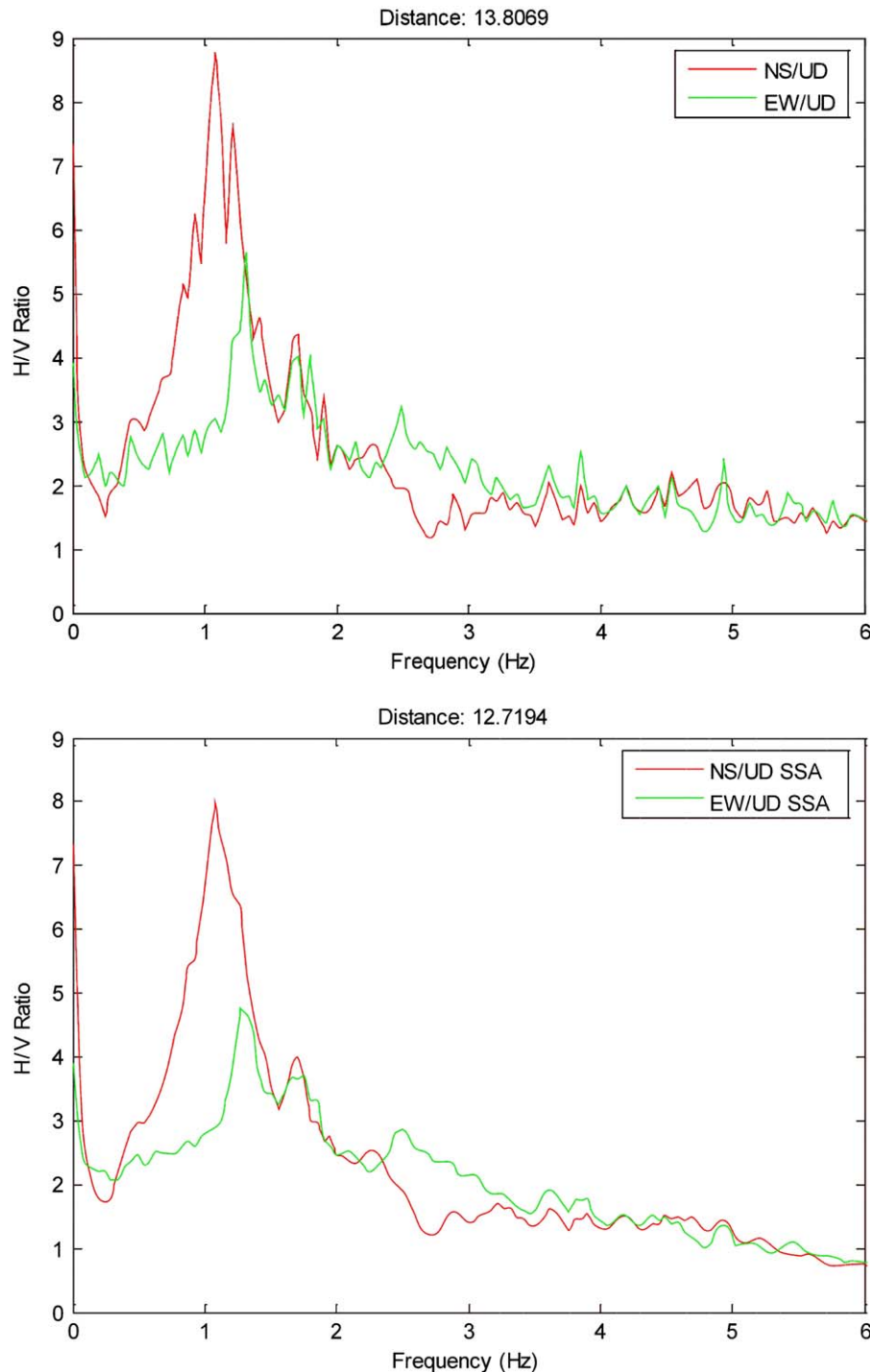


Fig. 4. Average spectral ratios for the two horizontal components over the vertical component for station 02 (a) without and (b) with the application of the SSA methodology.

two horizontal components and the vertical one for, a randomly selected station (05) before and after the application of SSA. It can be seen that the SSA results are generally more stable, eliminating the spurious peaks.

4.2. Application of the SSA technique on weak motion data

A dataset of 30 small earthquakes, $M_s < 3.3$, has been selected (Fig. 1, Table 1) in order to apply the SSA technique, on the HVSR

of the weak motion data. As the “matching” measure, the least squares sum was also chosen as in the case of microtremor data.

The first step of the procedure is to select an appropriate time window, including the S wave part, in order to perform the analysis. Then, we proceed with the decomposition of the signals using the SSA technique. After examining the components and the eigenvalues, an embedding dimension of $M=20$ was chosen for the specific dataset under consideration. A larger value for M was selected for the weak motion data, as there are more components with no negligible data present in these signals. Similarly to the way that the microtremor records were processed we obtain the

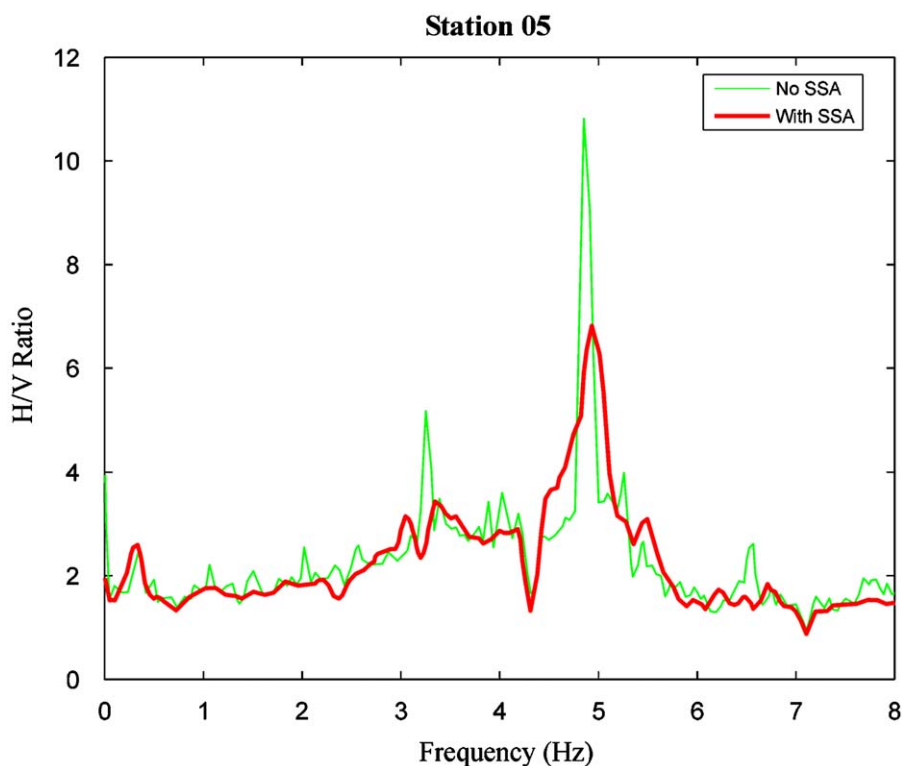


Fig. 5. Average spectral ratios for station 05 without (green line) SSA applied and with SSA applied (red line). For interpretation of the references to colour in this figure legend, the reader is referred to the web version of this article.

Table 1

Year	Month	Day	Hours	Minutes	Seconds	Latitude	Longitude	Depth	Magn
2002	Dec	8	20	2	50.30	37.85	21.14	20	2.8
2002	Dec	8	23	8	39.80	37.84	21.09	19	3.2
2002	Dec	9	18	8	34.00	37.82	21.14	16	3.3
2002	Dec	10	17	2	44.70	37.77	21.10	35	3
2002	Dec	11	18	19	5.00	37.83	21.13	17	3
2002	Dec	11	13	17	17.60	37.76	21.12	29	3.2
2002	Dec	11	15	45	20.20	37.76	21.12	26	3
2002	Dec	12	14	39	54.70	37.80	21.14	7	3
2002	Dec	13	2	29	46.00	37.81	21.13	16	3
2002	Dec	13	9	37	1.50	37.80	21.10	20	3.1
2002	Dec	13	8	48	29.70	37.80	21.09	24	3.1
2002	Dec	14	13	8	16.20	37.86	21.20	17	3.3
2002	Dec	14	5	48	35.90	37.84	21.10	35	3
2002	Dec	14	10	47	51.70	37.81	21.12	31	2.9
2002	Dec	15	11	46	23.20	37.84	21.21	16	2.9
2002	Dec	15	17	11	22.10	37.84	21.17	28	2.9
2002	Dec	16	18	6	37.80	37.86	21.24	13	2.8
2002	Dec	17	19	46	39.90	37.82	21.09	21	3.1
2002	Dec	19	6	39	54.20	37.87	21.16	18	2.9
2002	Dec	23	15	37	54.20	37.79	21.17	19	2.8
2002	Dec	23	17	49	5.70	37.84	21.19	16	2.9
2002	Dec	24	13	11	58.90	37.79	21.12	20	3.3
2002	Dec	25	3	29	17.60	37.86	21.17	34	2.9
2002	Dec	26	17	4	34.10	37.88	21.12	17	3.2
2002	Dec	30	7	35	17.10	37.75	21.20	8	2.8
2002	Dec	31	3	8	48.20	37.86	21.04	17	3.1
2003	Jan	3	10	57	31.60	37.84	21.15	25	2.8
2003	Jan	5	13	58	41.50	37.81	21.25	26	2.8
2003	Jan	6	20	6	23.30	37.85	21.22	15	3
2003	Jan	8	2	39	15.00	37.86	21.20	29	2.9

$S[SSA(x;M,q_1)]$, $S[SSA(y;M,q_2)]$ and $S[SSA(z;M,q_3)]$ taking care that the choice of the best triplet (q_1, q_2, q_3) minimizes the distance between the EW/UD and NS/UD distances. Fig. 6 shows the decomposition of the event of December 30, 2002 for station 05 (Table 1).

Fig. 7a, b presents the calculated spectral ratios, for NS and EW components, for station 05 for all the recorded weak events with and without SSA methodology respectively. The results are plotted in the same way as the microtremor ones in a semi logarithmic plot; dimensions are the same for all corresponding axis in Fig. 7a and b.

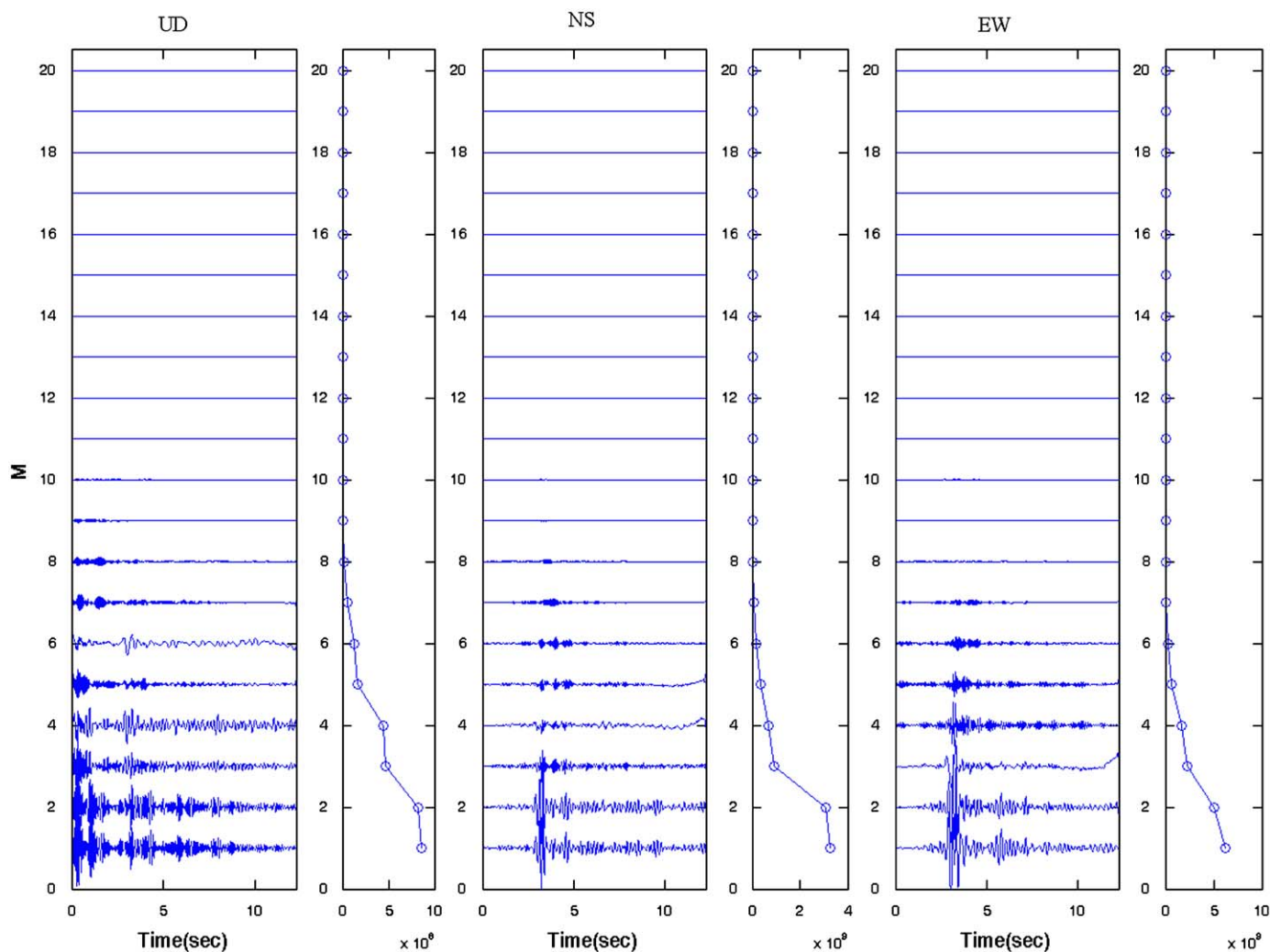


Fig. 6. SSA decomposition of the 3 components of the December 30, 2002 event as it was recorded in station 05 and its corresponding eigenvalues.

Although the SSA methodology does not eliminate some of the irregularly high peak values of the ratios it can reduce them significantly. This can be observed in Fig. 8 where the average ratios are compared, from both EW and NS components, for all the weak earthquakes selected without and with the application of the SSA methodology, for the previously selected station 05.

5. Results and discussion

The obtained results from all the stations (dominant frequencies and HVSRS) are combined in order to map the assessed local site effects properties. The maps presented include only the part inside the city of Vartholomio because only in this part the majority of the recording stations are located at sufficiently close distances.

In Figs. 9–12, the microtremor and weak motion results are interpolated in space and presented both without and with the application of the SSA methodology. Dominant frequency and corresponding HVSRS are plotted on the same diagram for each method. In these figures the dominant frequencies are colour coded while the spectral ratios are represented by the corresponding heights of the blocks. Figs. 9 and 10 present the results using the microtremor data without and with SSA applied, respectively. In the same way Figs. 11 and 12 show the results

from the weak motion data. Comparing these data we can conclude that the results without and with application of SSA; look very similar. But when comparing the results of the two datasets used (microtremors and weak events) the SSA results present a decreased discrepancy between the two.

There are small differences between the two results but the main features seem to be the same. The highest frequencies are found towards the southwestern part of the mapped area. Also both datasets agree that the values of the dominant frequencies become generally lower towards the eastern part. Fig. 13 a, b presents the difference in the results from the weak events minus the ones from microtremors, without (Fig. 13a) and after applying the SSA methodology (Fig. 13b). An improved convergence for the results of the two datasets can be seen. Without the SSA applied, the difference of the results between the two dataset ranges from -1.6 up to 0.88 Hz for the dominant frequencies and approximately 2.6 to 10.4 for the ratio. The differences in the SSA processed results remain unchanged for the frequencies but the differences between the ratio values are approximately between -1 and 4 .

Most authors favor an explanation of the difference between weak motion and microtremor HVSRS based on the polarization of Rayleigh waves, which should be more abundant in microtremors than in earthquakes [14]. If the microtremors consist primarily of surface waves generated at the sediment–bedrock interface, then

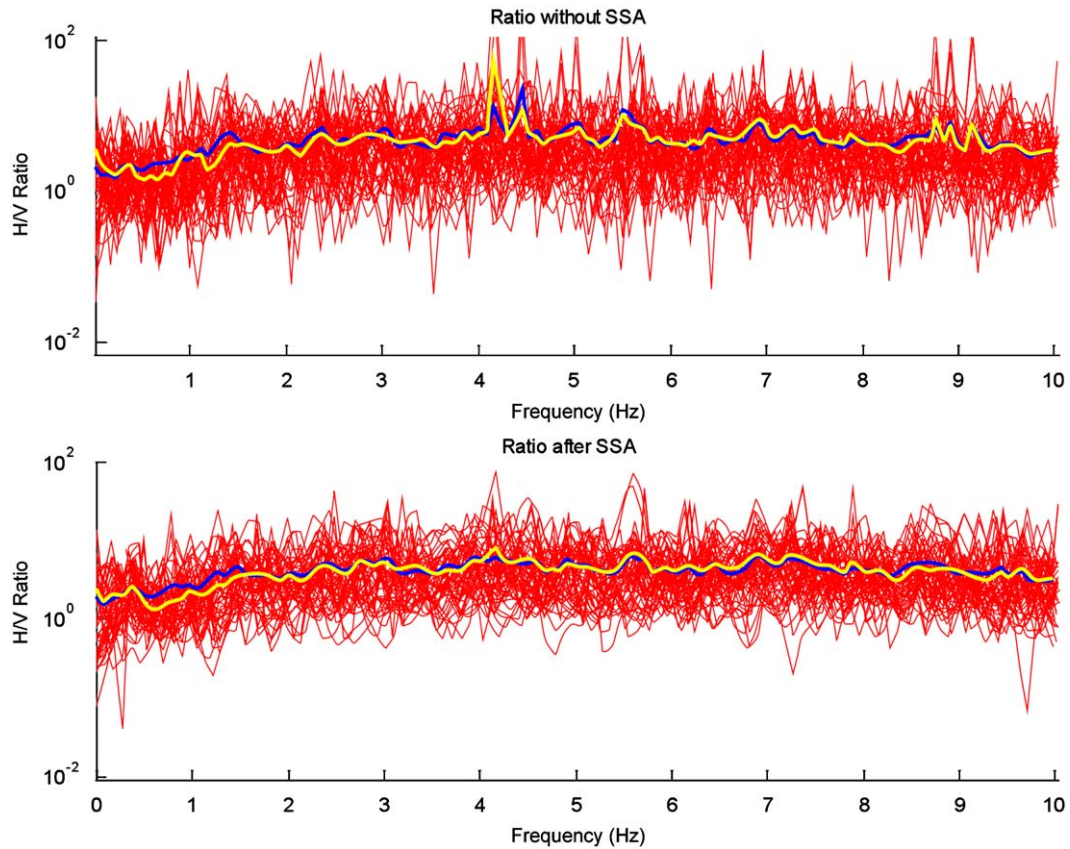


Fig. 7. Spectral ratios for station 05 for every event (both EW and NS in red) and the average ratios (blue NS, yellow EW) (a) without and (b) with the application of the SSA methodology. For interpretation of the references to colour in this figure legend, the reader is referred to the web version of this article.

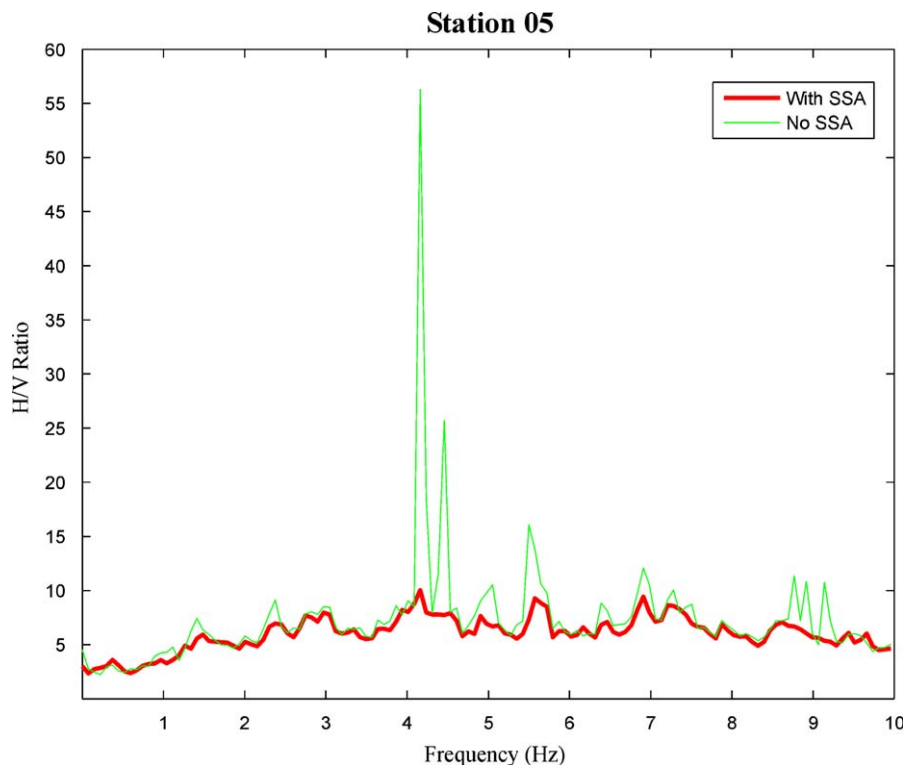


Fig. 8. Average spectral ratios for station 05 without (green line) and SSA with (red line) applied. For interpretation of the references to colour in this figure legend, the reader is referred to the web version of this article.

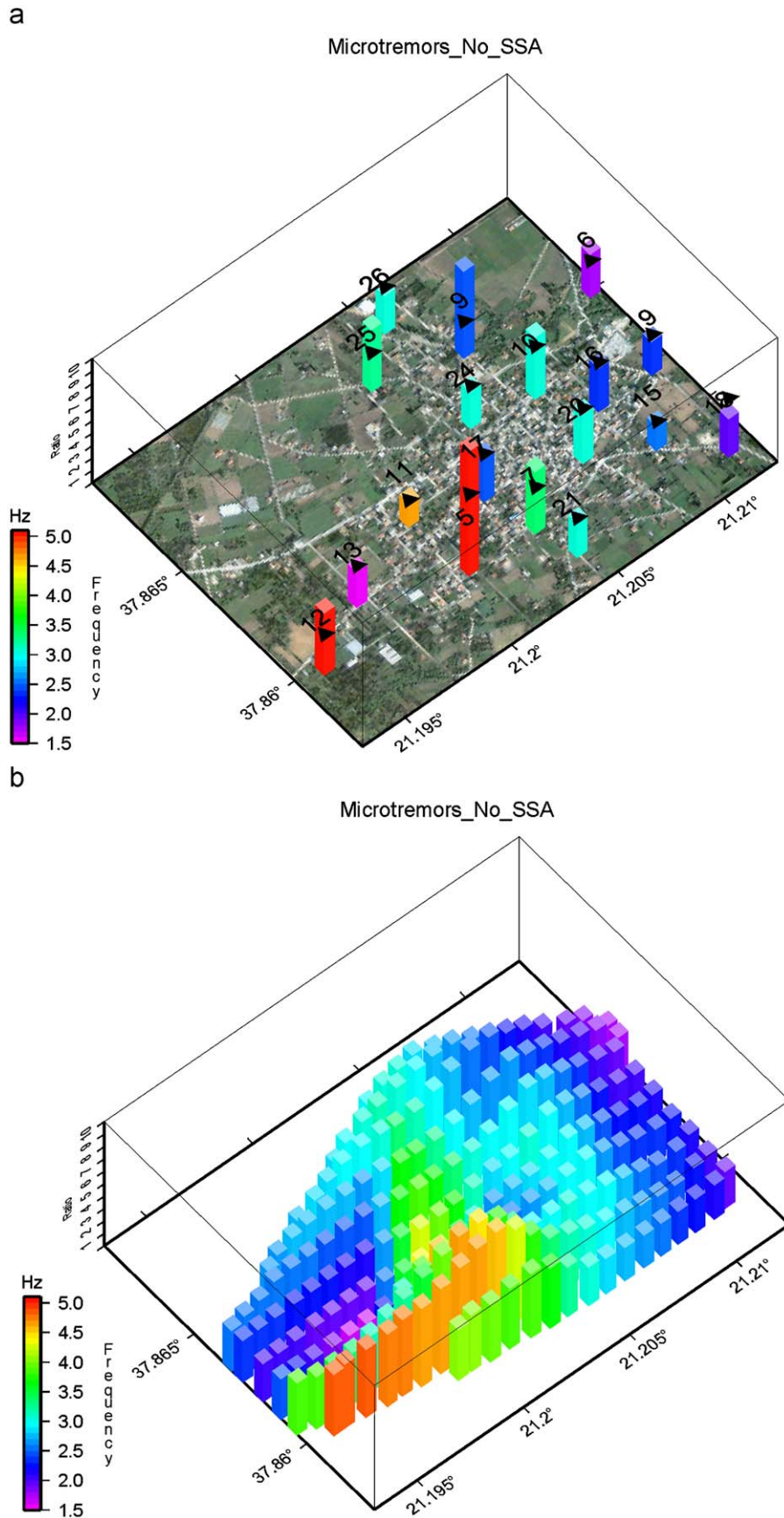


Fig. 9. Results for microtremor data. Without SSA method applied. (a) Results as observed on each station and (b) interpolated spatial distribution of HVRS. Colour code and block heights correspond to predominant frequencies and spectral amplitude ratios, respectively. For interpretation of the references to colour in this figure legend, the reader is referred to the web version of this article.

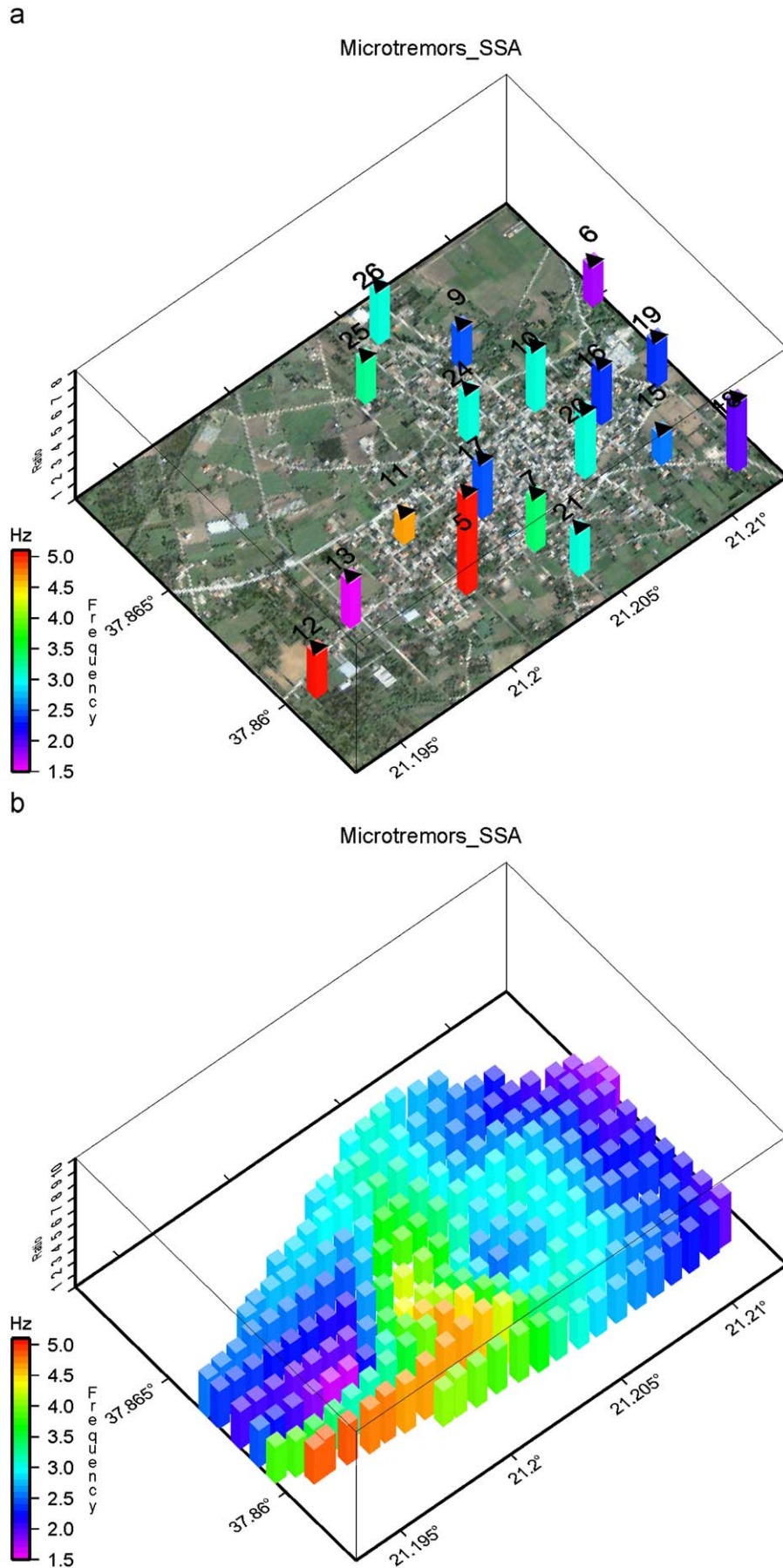


Fig. 10. Spatial distribution of HVRS results for microtremor data, by employing the SSA methodology. (a) Results as observed on every station and (b) interpolated spatial distribution of HVRS.

Please cite this article as: Tselentis G-A, Paraskevopoulos P. Site response analysis of Vartholomio W-Greece from singular spectrum analysis of microtremor and weak motion data. *Soil Dyn Earthquake Eng* (2010), doi:10.1016/j.soildyn.2009.12.011

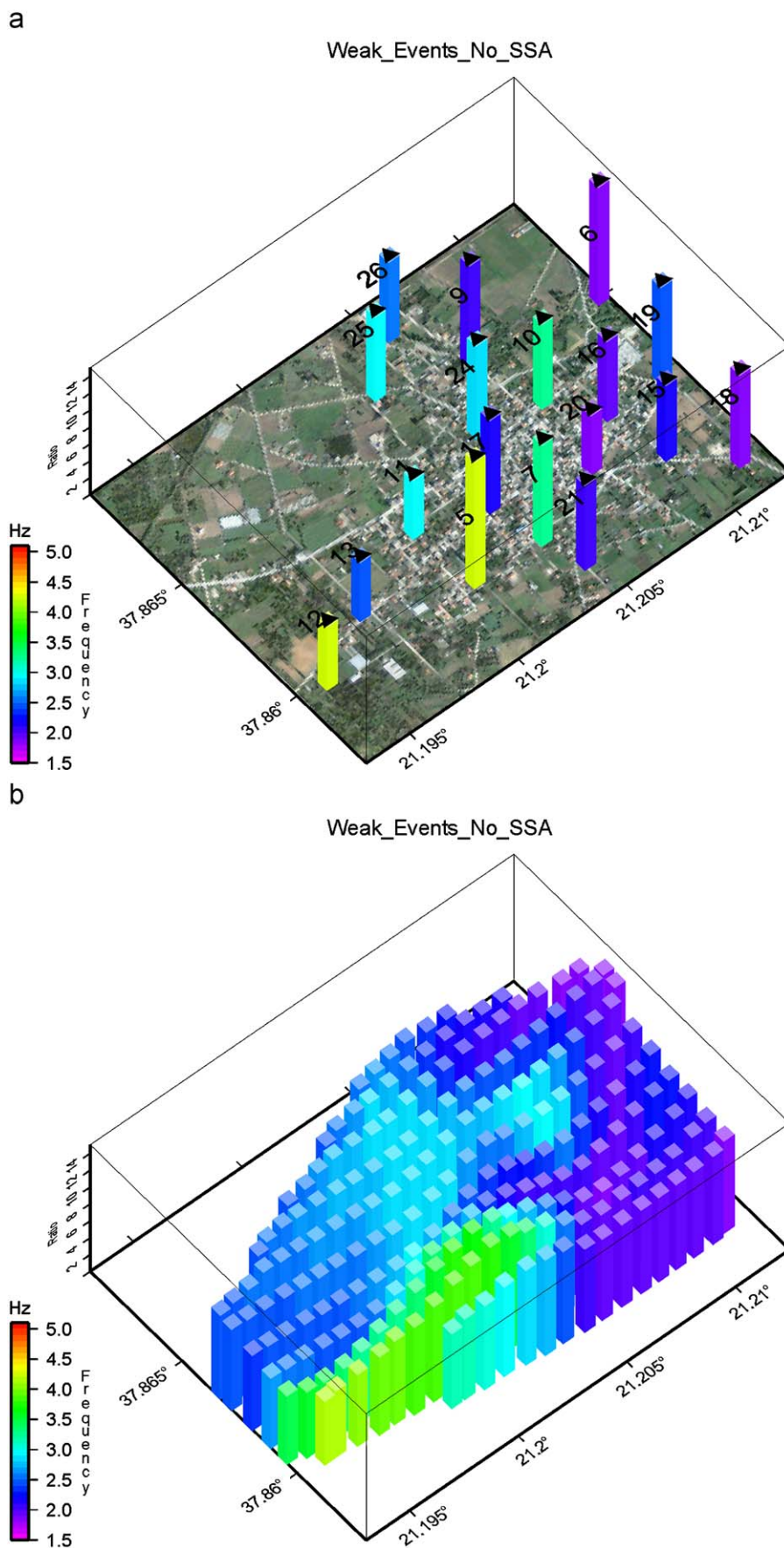


Fig. 11. Spatial distribution of HVRS results for microearthquake data without the SSA methodology. (a) Results as observed on every station and (b) interpolated spatial distribution of HVRS.

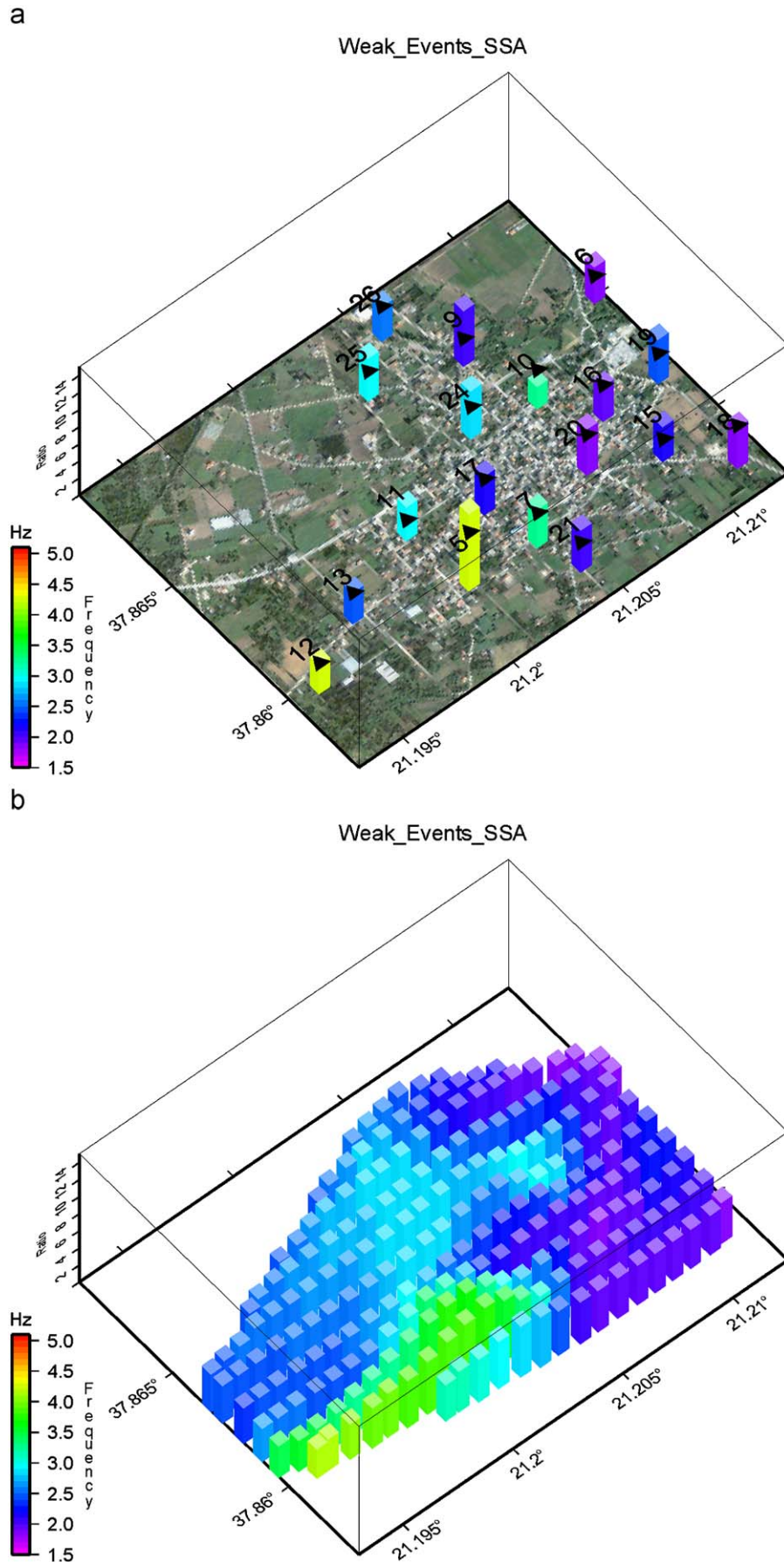


Fig. 12. Spatial distribution of HVRS results for microearthquake data with the SSA methodology. (a) Results as observed on every station and (b) interpolated spatial distribution of HVRS.

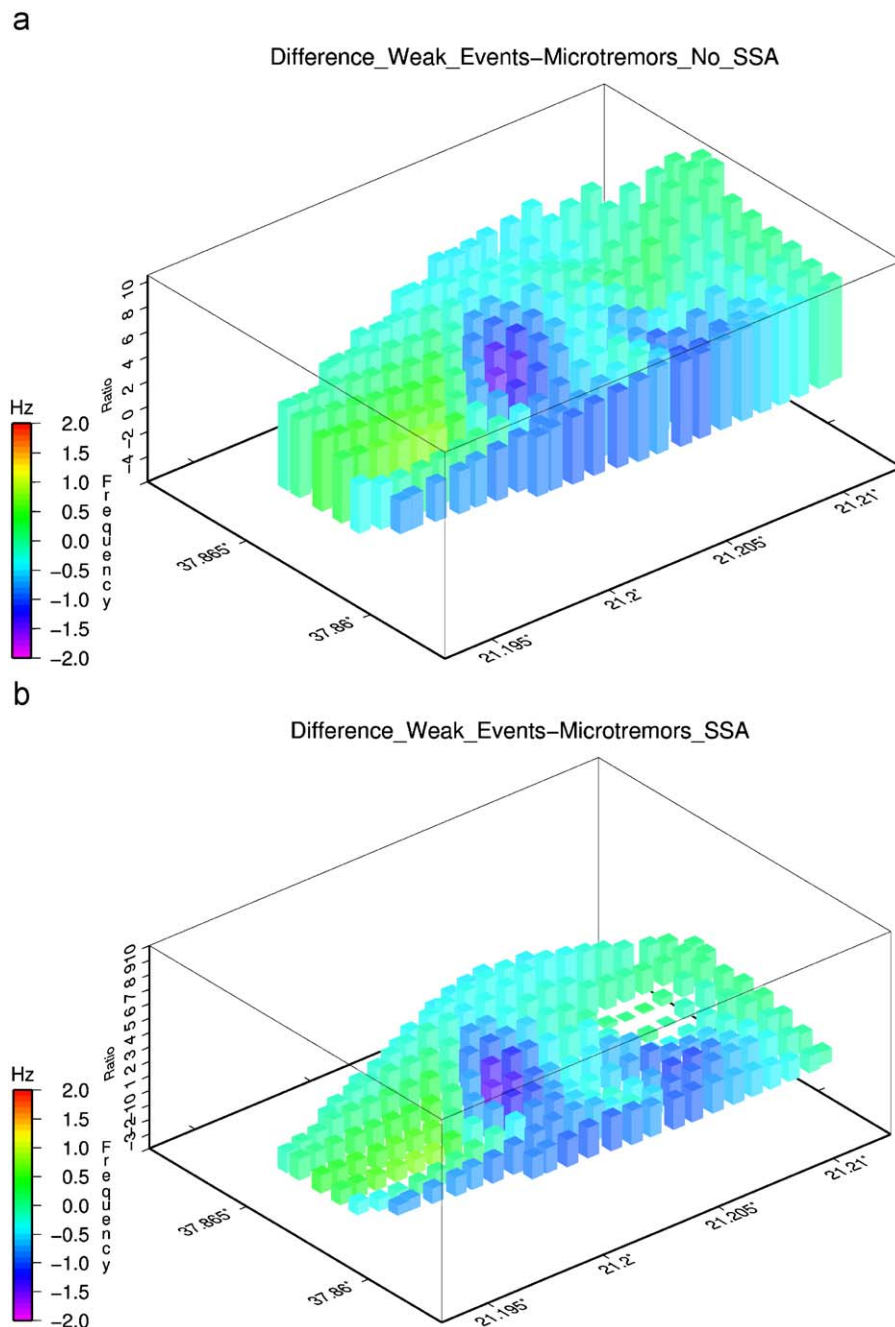


Fig. 13. Spatial distribution of the difference weak events—microtremors (a) without SSA and (b) with SSA applied.

the dominant period of these waves may not, in general, be expected to match precisely the fundamental period of the SH-wave resonance [19]. If the impedance contrast is strong enough to allow the surface waves to be trapped entirely within the sediment layer, then their dominant velocity and period will be close to that of an SH resonance in that layer. If the impedance contrast is weaker (as it was found from a seismic reflection survey), then the velocity of surface waves may partially reflect the higher shear wave velocity of the basement. In this case the dominant frequency of the microtremors is higher than that of the fundamental frequency of the shear wave resonance, something which can be seen in most parts of Fig. 13b.

The next step is to separate stations that present similar characteristics in their spectral ratios, performing a zonation of the study area. The method chosen was the automatic zonation

based on the similarity of spectral ratios proposed by [5,6]. The aim of this method is to optimally partition the dataset of measurements stations in a number of subsets whose points have maximal similarity.

The part of the spectral ratios used in all the cases was the same and ranged from 0 to 10 Hz. Assuming that the number of connected clusters (N_c) ranged from 2 up to 8 the genetic algorithm was run for each one of these values using 200 individuals per population; probability of crossover between 0.6 and 0.8 and probability of mutation between 0.001 and 0.02. Each run was completed after 1000 generations. The Bayesian information criterion (BIC) parameter was computed for every partition of measurement points.

The results when plotted in Figs. 14 (microtremors) and 15 (weak events) indicate the existence of 2 major zones even

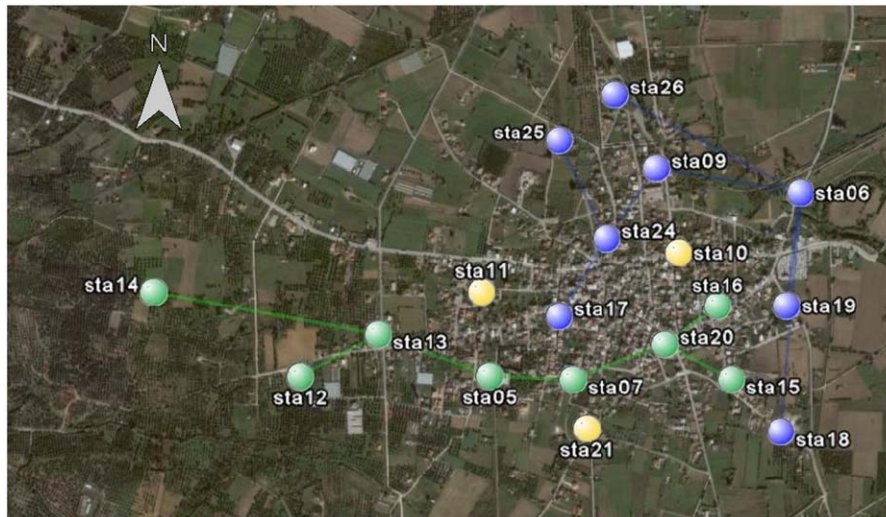


Fig. 14. Automatic zonation produced using the genetic algorithm for the microtremor data.

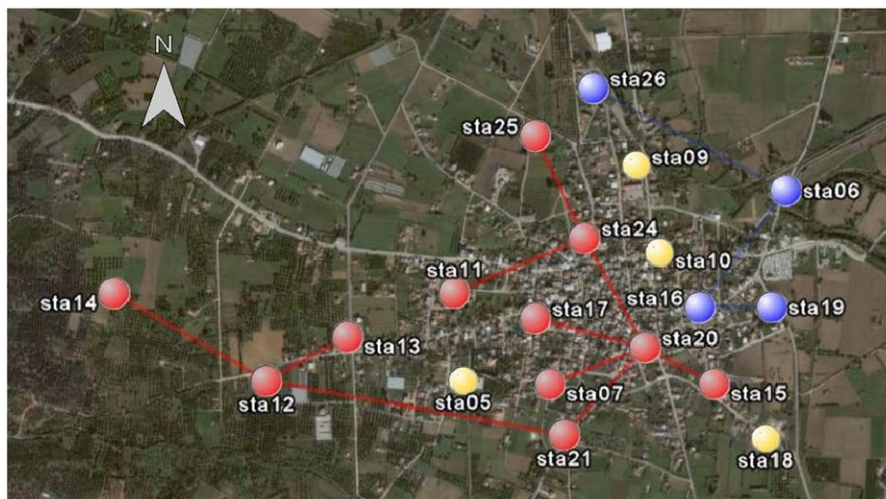


Fig. 15. Automatic zonation produced using the genetic algorithm for the microearthquake data.

though there seems to be a difference among the two datasets. There is one major zone towards the southwestern part of the city and a second one towards the northeastern part and also there are some stations (represented by the yellow dots) such as station 10 that are not included in any zone. The exact extents of these zones are different between the two datasets with the southwestern zone being larger in the zonation produced from the weak events results. Such differences can also be seen in the mapping of dominant frequencies and ratios of the two methods in Figs. 10 and 12. It could be that the zonation procedure does not work that well for the weak events as the spectral ratio seems to have more dispersion than the ones from the microtremors.

6. Conclusions

We have analyzed microtremor and weak earthquake recordings at a network of seismological stations installed within Vartholomio city. The SSA method is a promising tool for improving the results of the HVSR methods using microtremor as well as microearthquake recordings in the case where no significant lateral non-homogeneities exist. The same methodol-

ogy has been applied for both datasets and shown the ability of the SSA methodology to improve the ratios. Then using a genetic algorithm we performed an automatic optimal zonation of Vartholomio region using both microtremor and weak motion data. In the city of Vartholomio the results indicate the presence of two major zones. Also there are some stations that are outliers from these zones, maybe a result of special local conditions.

Uncited references

[17], [29], [33].

Acknowledgements

The authors would like to thank Pier Luigi Bragato for providing us with his GA zonation software. Anna Serpesisdiki and Efthimios Sokos are acknowledged for their helpful comments. Also, we would like to thank an anonymous reviewer for the interesting comments and remarks on the original manuscript.

References

- [1] Barazza F, Malisan P, Carniel R. Improvement of H/V technique by rotation of the coordinate system. *Commun Nonlinear Sci Numer Simul* 2009;14(1):182–93.
- [2] Bard P-Y. Microtremor measurements: a tool for site effect estimation? In: *Proceedings of the second international symposium on the effects of surface geology on seismic motion, Yokohama, Japan, vol. 3; 1998. p. 1251–79.*
- [3] Bard P-Y. The SESAME-Team. Report D23.12, Guidelines for the implementation of the H/V spectral ratio technique on ambient vibrations measurements, processing and interpretation in European Commission: Research General Directorate, Project No. EVG1-CT-2000-00026, SESAME, (2005), 62 pp. Available online at <<http://sesame-fp5.obs.ujf-grenoble.fr>> (last accessed April 2009).
- [4] Bettig B, Bard PY, Scherbaum F, Riepl J, Cotton F, Cornou C, Hatzfeld D. Analysis of dense array noise measurements using the modified spatial autocorrelation method (SPAC): application to the Grenoble area., *Boll Geofis Teor Appl* 2001;42(3–4):281–304.
- [5] Bragato PL, Bressan G. Automatic seismic zonation based on stress-field uniformity assessed from focal mechanisms. *Bull Seismol Soc Am* 2006;96:2050–2058.
- [6] Bragato PL, Laurenzano G, Barnaba C. Automatic zonation of urban areas based on the similarity of H/V spectral ratios. *Bull Seismol Soc Am* 2007;97:1404–12.
- [7] Broomhead DS, King GP. Extracting qualitative dynamics from experimental data. *Physica D* 1986;20:217–36.
- [8] Cara F, Cultera G, Azzara RM, De Rubeis V, Di Giulio G, Giammarinaro MS, et al. Microtremor measurements in the city of Palermo, Italy: analysis of the correlation with local geology and damage. *Bull Seismol Soc Am* 2008;98(3):1354–72.
- [9] Carniel R, Barazza F, Pascolo P. Improvement of Nakamura technique by singular spectrum analysis. *Soil Dyn Earthquake Eng* 2006;26:55–63.
- [10] Di Giulio G, Azzara RM, Cultrera G, Giammarinaro MS, Vallone P, Rovelli A. Effect of local geology on ground motion in the city of Palermo, Italy, as inferred from aftershocks of the September 9, 2002, M_w , 5.9. *Bull Seismol Soc Am* 2005;95(6):2328–41.
- [11] Duval AM, Vidal S, Meneroud J-P, Singer A, De Santis F, Ramos C, et al. Cracas, Venezuela, site effects determination with microtremors. *Pure Appl Geophys* 2001;158:2513–23.
- [12] Elsner AA, Tsonis AA. *Singular spectrum analysis: a new tool in time series analysis.* New York: Plenum Press; 1996.
- [13] Fäh D. Microzonation of the city of Basel. *J Seismol* 1997;1(1):87–102.
- [14] Field EH, Jacob KH. A comparison and test of various site-response estimation techniques, including three that are not reference-site dependent. *Bull Seismol Soc Am* 1995;85:1127–43.
- [15] Gitterman Y, Zaslavsky Y, Shapira A, Shtivelman V. Empirical siteresponse evaluations: case studies in Israel. *Soil Dyn Earthq Eng* 1996;15:447–63.
- [16] Golyandina N, Osipov E. The “Caterpillar”-SSA method for analysis of time series with missing values. *J Stat Plann Infer* 2007;137(8):2642–53.
- [17] Hough SE, Seeber L, Rovelli A, Malagnini L, DeCesare A, Selvaggi G, Lerner-Lam A. Ambient noise and weak motion excitation of sediment resonances: results from the Tiber Valley, Italy. *Bull Seismol Soc Am* 1992;82:1186–205.
- [18] Lachet C, Hatzfeld D, Bard P-Y, Theodulidis N, Papaioannou C, Savvaidis A. Site effects and microzonation in the city of Thessaloniki (Greece): comparison of different approaches. *Bull Seismol Soc Am* 1996;86:1692–703.
- [19] Langston CA. Structure under Mount Rainier, Washington, inferred from teleseismic body waves. *J Geophys Res* 1979;84:4749–62.
- [20] Lebrun B, Hatzfeld D, Bard P-Y. A site effect study in urban area: experimental results in Grenoble (France). *Pure Appl Geophys* 2001;158:2543–57.
- [21] Le Pichon X, Chamot-Rooke N, Lallemand S, Noomen R, Veis G. Geodetic determination of the Kinematics of Central Greece with respect to Europe. *J Geophys Res* 1995;100(B7):12675–90.
- [22] Lekkas E, Papanikolaou D, Fountoulis I. Neotectonic map of Greece. Sheets Pyrgos and Tropea. University of Athens; 1992 Comment: 120 pp.
- [23] Mucciarelli M, Gallipoli MR, Arcieri M. The stability of the horizontal-to-vertical spectral ratio of triggered noise and earthquake recordings. *Bull Seismol Soc Am* 2003;93(3):1407–12.
- [24] Nakamura Y. A method for dynamic characteristics estimations of subsurface using microtremors on the ground surface. *Q Rep RTRI Jpn* 1989;30:25–33.
- [25] Nakamura Y. Real-time information systems for hazards mitigation. In: *Proceedings of the 11th world conference on earthquake engineering, Acapulco, Mexico; 1996.*
- [26] Nakamura Y. Clear identification of fundamental idea of Nakamura’s technique and its applications. In: *Proceedings of the 12th world conference on earthquake engineering, Auckland, New Zealand; 2000.*
- [27] Nogoshi M, Igarashi T. On the amplitude characteristics of microtremor (part 2). *J Seismol Soc Jpn* 1971;24:26–40. (in Japanese with English abstract).
- [28] Palus M, Novotna D. Detecting modes with nontrivial dynamics embedded in colored noise: enhanced Monte Carlo SSA and the case of climate oscillations. *Phys Lett A* 1998;248(2–4):191–202.
- [29] Panou A, Theodulidis N, Hadzidimitriou P, Savvaidis A, Papazachos C. Reliability of ambient noise horizontal to vertical spectral ratio in urban environments: The case of Thessaloniki city (Northern Greece). *Pure Appl Geophys* 2005;162(5):891–912.
- [30] Reinoso E, Ordaz M. Spectral ratios for Mexico City from free-field recordings. *Earthquake Spectra* 1999;15:273.
- [31] Riepl J, Bard P-Y, Hatzfeld D, Papaioannou C, Nechtschein S. Detailed evaluation of site response estimation methods across and along the sedimentary valley of Volvi (EURO-SEISTEST). *Bull Seismol Soc Am* 1998;88(2):488–502.
- [32] Seekins L, Wenneberg L, Margheriti L, Liu H-P. Site amplification at five locations in San Francisco, California: a comparison of S waves, codas, and microtremors. *Bull Seismol Soc Am* 1996;86(3):627–35.
- [33] Teves-Costa P, Almeida IM, Silva PL. Microzonation of Lisbon: 1D theoretical approach. *Pure Appl Geophys* 2001;158:2579–96.
- [34] Theodulidis N, Bard P-Y, Archuleta RJ, Bouchon M. Horizontal to vertical spectral ratio and geological conditions: the case of Garner Valley downhole array in Southern California. *Bull Seismol Soc Am* 1996;86:306–19.
- [35] Tselentis GA, Vasiliou I, Lekkas E, Roubos D, Sokos E. Site specific design strong motions at the city of Vartholomio—Greece. In: *Proceedings of the third conference of geotechnical engineering, Patras, vol I, 1998. p. 567–74.*
- [36] Udvardi FE, Trifunac MD. Comparison of earthquake and microtremor ground motions in El Centro, California. *Bull Seismol Soc Am* 1973;63:1227–53.
- [37] Vautard P, Yiou P, Ghil M. Singular spectrum analysis: a toolkit for short, noisy chaotic signals. *Physica D* 1992;58:95–126.
- [38] Yamazaki F, Ansary MA. Horizontal-to-vertical spectrum ratio of earthquake ground motion for site characterization. *Earthquake Eng Struct Dyn* 1997;26:671–689.
- [39] Zaré M, Bard P-Y, Ghafory-Ashtiany M. Site categorization for the Iranian strong motion network. *Soil Dyn Earthquake Eng* 1999;18:101–23.